

Hybrid Single-Ion Atomic-Ensemble Node for High-Rate Remote Entanglement Generation

Benedikt Tissot,^{1,*} Soubhadra Maiti,^{2,3} Emil R. Hellebek,¹ and Anders Søndberg Sørensen^{1,†}

¹Center for Hybrid Quantum Networks (Hy-Q), Niels Bohr Institute,

University of Copenhagen, Jagtvej 155A, DK-2200 Copenhagen, Denmark

²QuTech, Delft University of Technology, Lorentzweg 1, 2628 CJ Delft, The Netherlands

³EEMCS, Quantum Computer Science, Delft University of Technology, Mekelweg 4, 2628 CD Delft, The Netherlands

Different quantum systems possess different favorable qualities. On the one hand, ensemble-based quantum memories are suited for fast multiplexed long-range entanglement generation. On the other hand, single-atomic systems provide access to gates for processing of information. Both of those can provide advantages for high-rate entanglement generation within quantum networks. We develop a hybrid architecture that takes advantage of these properties by combining trapped-ion nodes and nodes comprised of spontaneous parametric down conversion photon pair sources and absorptive memories based on rare-earth ion ensembles. To this end, we solve the central challenge of matching the different bandwidths of photons emitted by those systems in an initial entanglement-generation step. This enables the parallel execution of multiple probabilistic tasks in the initial stage. We show that our approach can lead to a significant speed-up for the fundamental task of creating ion-ion entanglement over hundreds of kilometers in a quantum network.

Long-range entanglement generation is central to building a quantum internet [1, 2]. Therein, the entanglement can be used for secure communication [3–6], enhanced sensing [7, 8], distributed computing [9], as well as fundamental physics experiments like the violation of Bell-inequalities [10–14]. While entanglement generation between separate matter systems has been demonstrated in various physical implementations – e.g., between atomic ensembles [15–17], trapped ions [18–20], color centers in solids [21–23], and rare earth ions [24–26] – high-rate entanglement generation over hundreds of kilometers remains a challenge.

Trapped ions are a favorable candidate for quantum network nodes, because they are established computational qubits featuring high fidelity quantum gates [27, 28] and long coherence times [29]. Local one- and two-qubit gates allow implementing network protocols, e.g., repeaters, dividing long-distance entanglement into smaller segments to overcome exponential loss in optical fibers [30–32]. An outstanding problem, however, is that the entanglement generation rate is slow over long distances.

To achieve a faster rate, one can employ multiplexing, which boosts the rate of possible entanglement generation attempts of a single qubit from c/L over a distance L with c being the speed of light to Nc/L for N qubits [26, 33]. Nodes combining photon pair sources based on spontaneous parametric down conversion and an absorptive memory using a rare-earth ion doped crystal (SPDC+M) have demonstrated high multiplexing capabilities and feature high duty cycles [24–26, 33, 34] and long storage durations [35, 36]. Single SPDC+M nodes have been shown to support more than 1000 modes [37], which is more feasible and cost-effective than trying to link 1000 trapped ions in parallel. Although the high number of memory modes makes ensemble nodes ideal

for entanglement generation over an elementary link, due to the absence of deterministic gates, information has to be transferred to other systems for processing. Repeaters can be implemented using linear optics [31], but in this case, the probabilistic nature of the entanglement swapping (henceforth swap for brevity) limits the entanglement generation rate for long distances [33].

In this letter, we propose a hybrid architecture tailored towards high-rate long-distance entanglement generation by uniting an SPDC+M backbone (BB) and trapped-ion edge-nodes (EN). Both systems can be entangled with photons with high fidelity [38–41], which can interface the systems. However, this is challenged by the mismatch of the intrinsically *narrow* bandwidth of photons emitted by ions, and the *broad-band* nature of SPDC photons. One approach to overcome this is photon (re-)shaping [42–45] within a final swap between the ion and the memory [46]. We propose a novel approach where we instead use the multi-mode nature of SPDC photon pairs by matching the photon correlation time of the SPDC to the broad bandwidth of the quantum memory, while SPDC is modulated proportional to the slowly varying temporal mode of the photon emitted by the ion. Thereby we overcome the orders of magnitude different emission time-scales (SPDC ~ 100 ns [24] and trapped ions in a cavity ~ 10 μ s [20, 47]). Furthermore, our approach exploits short-range connections for the (likely) most inefficient links between the ions and the ensembles. As a result, these links can be generated at a high repetition rate to compensate for the limited probability.. The long-range entanglement, which has to be performed at a slower rate due to the long communication time, is on the other hand enhanced by ensemble multiplexing. Performing the matching and long-range generation simultaneously furthermore avoids unnecessary idle time. With this method, rapid long-range entanglement can be established in a full network

of links between different trapped ions. Local deterministic entanglement swaps between the ions can then further extend the range and complexity of the network.

We focus on long-distance entanglement generation and thus consider a single-click scheme, but note that for shorter links or efficient ensemble memories, two-click [31, 32, 48] or reflection-based [49, 50] protocols might be beneficial. The *entanglement generation protocol* is illustrated in Fig. 1(d) and (e), and can be summarized in four steps. It proceeds by (i) simultaneously generating entanglement links using single-click heralding between ions and memories locally at ENs [Fig. 1(a)] and between BB memories over a long distance L [Fig. 1(b)]. (ii) As soon as neighboring BB and EN links are ready, entanglement is swapped between them by heralding on a single click after releasing the photons from the memories [Fig. 1(c)]. Finally (iii) another optical swap between memories at the central repeater, connects the two halves. We include a repeater in the center of the fundamental link, because parallelization allows the additional swap to extend the distance, without significantly decreasing the success rate [51]. Alternatively, without the central repeater, a final swap can be performed between the BB and the remaining EN. Upon successfully heralding every step, an ion-ion entangled link is achieved. The *last part* (iv) is purification to distill two ion-ion links into a single link with enhanced fidelity, see Fig. 1(e). It proceeds by preparing two ion-ion links using the steps above and performing a CNOT gate between the local ions. Measurement of both target ions in state $|1\rangle$ heralds the purification of the ion-ion entanglement, see Fig. 1(e). This post-selection helps in suppressing events where the memories did not store any photons while retaining the better scaling of single-click protocols with the (long-distance) fiber losses [31–33, 52, 53]. Although the single-click protocol inherently relies on phase stability [31, 32, 54], the purification can reduce the sensitivity to such fluctuations if the phase is stable between two successful entanglement generation events [54].

A central part of our proposal is a method to bridge the different intrinsic time scales of the trapped ions and BB memories. To describe this, we model the matter systems using the combined photonic and matter state immediately after the emission. To implement a single-click protocol [32], we consider the *ions* to emit photons conditioned on the internal state,

$$|\Psi_a\rangle = \left[\alpha_0 |0\rangle + \alpha_1 |1\rangle \int_{\mathbb{R}} dt \nu(t) a^\dagger(t) \right] |\emptyset_a\rangle, \quad (1)$$

with the matter states $|0\rangle$ and $|1\rangle$, the emission amplitude α_1 ($\alpha_0 = \sqrt{1 - |\alpha_1|^2}$), the photonic creation operator a^\dagger with the channel vacuum state $|\emptyset_a\rangle$, and the normalized temporal mode function $\nu(t)$ of duration T_a . A state of this form can, e.g., be generated using stimulated Raman emission [45, 55, 56].

For (quasi) continuous driving of an SPDC successful events are typically defined by the detection of a photon in one arm in a time window around the detection time in the other arm. To describe this we divide the time interval into time bins corresponding to the acceptance interval. We take the SPDC+M state within a time-bin as the multi-modal state

$$|\Psi_b\rangle = \left[\beta_0 + \beta_1 \int_{\mathbb{R}^2} dt dt' \mu(t) F(t, t') b^\dagger(t) c^\dagger(t') \right. \\ \left. + \beta_2 \int_{\mathbb{R}^4} d\vec{t} \mu(t_1) \mu(t_2) G(\vec{t}) b^\dagger(t_1) b^\dagger(t_2) c^\dagger(t_3) c^\dagger(t_4) \right] |\emptyset\rangle, \quad (2)$$

based on the detailed model developed in Ref. [57]. The operator b^\dagger (c^\dagger) corresponds to creating a photon in the channel connected with the BS and detectors (the memory), see Fig. 1. Here β_1 (β_2) denote the single (two) photon emission amplitude within a time-bin. The vacuum state $|\emptyset\rangle$ has the amplitude β_0 . The temporal mode μ captures the overall shape of the first detected photon (in the b mode), while the multi-modal and multi-photon character is contained in the multi-time-dependence of the (double) pair correlation function $F(t, t')$ [$G(\vec{t})$]. The correlation time T_c between the photons of a pair corresponds to the width of $F(t, t')$ in the time difference $t' - t$. As the aim is to store most of the photon while avoiding storage of uncorrelated photons, we choose the acceptance interval and therefore the time-bin to be a few times the correlation time of $F(t, t')$ (see Fig. 2) but shorter than the much longer ion photon duration.

For the optical entanglement generation, as well as the probabilistic swaps, we consider a setup that combines two input channels using a 50:50 beamsplitter with the two beamsplitter outputs terminating in detectors, see Fig. 1 (a)–(c). For both entanglement generation and swapping we use a single click to herald success, and we model the optics for channels a and b using $a^\dagger \rightarrow \sqrt{\eta/2}(d_+^\dagger + d_-^\dagger) + \sqrt{1-\eta}a_L^\dagger$ and $b^\dagger \rightarrow \sqrt{\eta'/2}(d_+^\dagger - d_-^\dagger) + \sqrt{1-\eta'}b_L^\dagger$, see Ref. [54] for additional details. Here, the combined efficiencies η and η' account for all losses from emission to the detection of a click and can account for differences in the branches before the beamsplitter, e.g., frequency conversion [47, 58] in one of the channels. The operators d_\pm annihilate a photon at one of the detectors and the operators a_L and b_L are annihilation operators of the loss channels. Losses in the memory channel are treated analogously and we denote the efficiency up to detection (after release during a swap) as η_m .

We present a general detection model in Ref. [54] and for simplicity here consider a sufficiently narrow temporal resolution and no dead-time such that we take the temporal modes as constant within the detection window and the detectors as photon-number-resolving. Thus, heralding on a single click ideally corresponds to post-selecting on only one detector channel \pm containing a single photon within the detector resolution T around the click time t_c , i.e., a projection of the detector channels onto

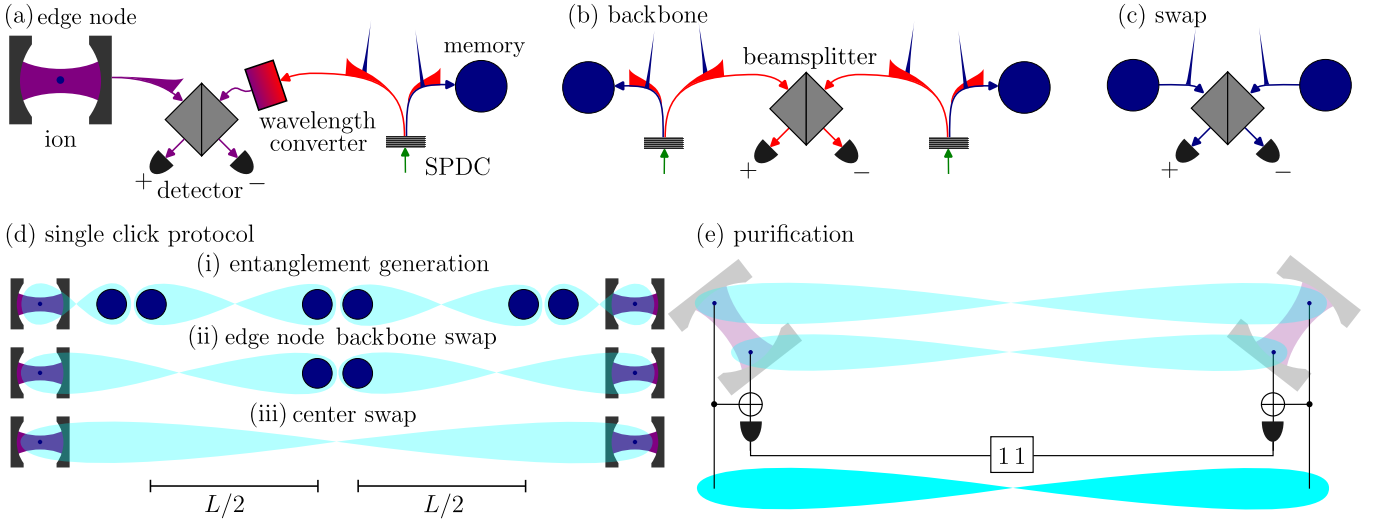


FIG. 1. Sketch of the protocol and device setups. (a) The edge-nodes (EN) consist of a trapped ion (in a cavity) and a spontaneous parametric down conversion source with attached multi-mode memory (SPDC+M) connected by fiber optics. After wavelength converting the SPDC photon to match the ion wavelength, the photons are interfered on a beamsplitter (BS) and measured with heralding detectors labeled \pm . (b) The backbone is composed entirely of SPDC+M nodes interconnected by optical fibers and heralding detectors. (c) Memory-memory swaps are also implemented using fiber optics, BS, and heralding detectors. (d) Ion-ion entanglement generation is generated using a single-click protocol over the long distance L spanned by the backbone network. To this end, (i) backbone and edge-node entanglement is generated in parallel using the setups depicted in (a),(b); (ii) a swap (c) is performed between the edge-nodes and the closest backbone link. (iii) Finally, a swap in the center links the ions. (e) Performing the single-click scheme twice enables the use of purification. We consider a purification where local CNOTs followed by measurement of both controlled systems in $|1\rangle$ post-selects a Bell state of higher fidelity.

$\int_{t_c-T/2}^{t_c+T/2} dt d_{\pm}^{\dagger}(t) |\emptyset_+\rangle |\emptyset_-\rangle$ with the annihilation operator d_{\pm} and vacuum state $|\emptyset_{\pm}\rangle$ of detector channel \pm . Additionally, we model dark counts as the detection of a click event despite the corresponding detection channel being in vacuum.

While variances of the phase can be accounted for within our model by making the temporal modes complex functions, we assume phase stability or active stabilization of the setup (required by all single-click protocols [31, 32, 54]) and use the modes as positive functions in the following. Additionally, we calculate the EN and BB state perturbatively to first order in emission probabilities and the ratio of dark count to successful detections. Within the EN links, we use the multi-mode nature of the SPDC photon pairs before the heralding to match the photon flux to the ion emission, as illustrated in Fig. 2. Slowly modulating the drive strength of the SPDC modulates the photon flux (corresponding to the slow envelopes $\mu(t)$ of the time-bins). This allows matching the temporal mode of the ion emission and thereby overcoming the challenge of matching a broadband ensemble system to the ion. Because the SPDCs within the ENs match the longer ion emission time-scale, we consider them to be weakly driven and thus to emit uncorrelated pairs [59]. The broadband nature of the SPDC emission then leads to a temporally narrow photon stored in the memory upon detection of the heralding click. The click time is used to filter and or precisely time the release of photons

from neighboring memories for entanglement swapping [60, 61]. This makes the heralded state insensitive to memory photons outside the acceptance interval and increasing the drive strength thereby suppresses part of the effect of losses in the SPDC channel. We therefore propose to place the frequency conversion, required to match the wavelengths of the systems, in the SPDC channel. To this end we express $\eta' = \eta'_0 \eta_{\text{FC}}$ with an intrinsic efficiency η'_0 and the frequency conversion efficiency η_{FC} .

The state heralded by a single click in port \pm during the ion photon duration after tracing out the photon loss and detection channels is

$$\rho_{\pm}^{\text{EN}} \approx (A_0 |0\rangle\langle 0| + A'_1 |1\rangle\langle 1|) |\emptyset\rangle\langle\emptyset| + A_1 |\varphi_{\pm}\rangle\langle\varphi_{\pm}| + A_2 |1\rangle\langle 1| |t_c\rangle\langle t_c|, \quad (3)$$

with the generated target state $|\varphi_{\pm}\rangle = \cos\theta |1\rangle |\emptyset\rangle \pm \sin\theta |0\rangle |t_c\rangle$ with $\tan^2\theta = \frac{\eta'_0 \eta_m |\mu(t_c) \alpha_0 \beta_1|^2}{\eta' |\nu(t_c) \alpha_1 \beta_0|^2}$. We highlight that matching the slowly varying SPDC temporal mode to the temporal mode of the ion photon makes θ independent of the click time. The first ket $|k\rangle$ ($k = 0, 1$) denote the atomic state and the second ket the memory photon state in vacuum $|\emptyset\rangle$ or with a single excitation stored in the multi-mode memory $|t_c\rangle = \int_{\mathbb{R}} dt F(t_c, t) c^{\dagger} |\emptyset\rangle$ conditioned on the detection of a click at time t_c . The elements of the density matrix up to mixed first order are given in Ref. [54] and only $A_0 \approx (1 - \eta_m) \frac{\tan^2\theta}{\eta_m + \tan^2\theta}$ and $A_1 \approx \eta_m \frac{1 + \tan^2\theta}{\eta_m + \tan^2\theta}$ have a non-perturbative contribution

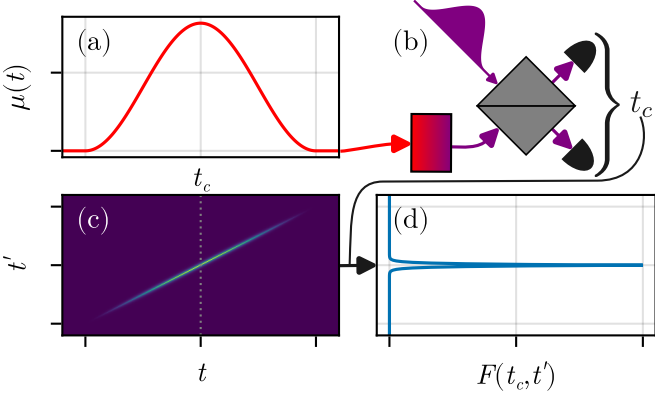


FIG. 2. Matching the SPDC and ion photon flux within the edge-nodes. The correlation function of the photon pair $\mu(t)F(t, t')$ of all time-bins (c) emitted by the SPDC is split into a slowly varying envelope $\mu(t)$ (a) that we can use to match to the atomic photon $\nu(t)$ (b). Conditioned on the heralding click, (d) a short photon is stored within one of the time-bins of the multi-mode (ensemble) memory unless it is lost. For illustration we use $T_a/T_c = 100$.

in magnitude.

The success probability corresponding to the probability of only detecting a single click at any time t_c during the ion-pulse duration T_a in either detector \pm has the leading contribution

$$P_{EN} \approx \eta |\alpha_1|^2 \left(1 + \frac{\tan^2 \theta}{\eta_m} \right), \quad (4)$$

if the slowly varying SPDC envelope ideally matches the ion emission $|\mu(t_c)|^2 = |\nu(t_c)|^2 N$. For simplicity, we assume that the N time-bins all have the same emission probability $|\beta_1|^2$. In addition to the leading order, we also account for the effect of dark counts and second order terms in the emission probability in the simulations.

In parallel to the link generation with the ENs, a multiplexed single-click protocol is performed in the BB. These types of protocols are well established [33, 52], and we provide a model analogous to the ENs for the BB in Ref. [54]. Due to the different constraints of the link generation between BB and EN, the SPDC emission probabilities within EN ($|\beta_1|^2$) and BB ($|\gamma_1|^2$) are chosen independently.

Ideally, the click times and memory storage are used to re-emit the stored photons simultaneously for the optical swaps. Therefore, we assume the memory photons share the same shape $f(t) = F(0, t)$. As we already included all losses in the generation step of our model to calculate the entanglement swaps, we can straightforwardly apply the same detection model used for the generation step. The first swap (between EN and BB) ideally extends the state $|\varphi_{\pm}\rangle$ to be between the ion and the next memory [see Fig. 1(d)]. Within the perturbative approximation considered here, we find the final density matrix of the

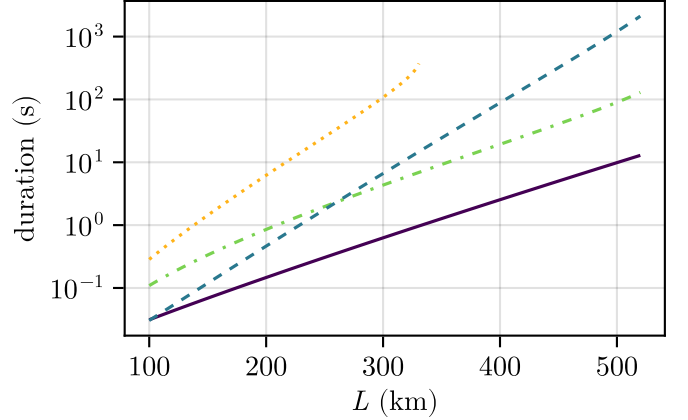


FIG. 3. Duration to prepare a Bell state with 99% fidelity as a function of length comparing different protocols. The dotted yellow (dash dotted green) line corresponds to direct ion-ion entanglement generation using a single-click protocol (with an ion node in the center as a repeater). The dashed blue (solid purple) lines correspond to the protocol proposed in this work without (with) a central multi-mode repeater. We take the efficiencies $\eta_m = 0.8$, $\eta = \eta'_0 = \eta_{FC} = 0.9$, and $\eta' = \eta'_0 \eta_{FC}$. The BB has $N_{BB} = 1000$ multiplexing modes and an efficiency $\eta_{BB} = \eta'_0 \eta_F (L/n)$ where $\eta_F(l)$ is the fiber transmission efficiency for distance l and an attenuation of 0.2 dB/km and $n = 4(2)$ with(out) a repeater. For direct ion-ion generation the photon efficiency is $\eta_{FC} \eta \eta_F(L)$. Furthermore we use a dark-count rate of 10^{-3} Hz, a pulse duration of the ions of 10 μ s, a acceptance window in the backbone of 1 μ s (i.e., $N = 10$), correlation duration of 100 ns, a detector resolution of 1 ns, and the speed of light in fiber as 2/3 the vacuum speed of light.

ions

$$\rho = (\pm \alpha |0, 1\rangle \langle 1, 0| + H.c.) + \sum_{k, l=0, 1} D_{k, l} |k, l\rangle \langle k, l|, \quad (5)$$

where \pm is the product of all the detectors that have clicked. The detailed calculation and density matrix elements $D_{k, l}$ and α can be found in Ref. [54]. Ideally, the only non-zero elements are $D_{0, 1} = D_{1, 0} = \alpha = 1/2$, which corresponds to the Bell states $\sqrt{2} |\Psi_{\pm}\rangle = |0, 1\rangle \pm |1, 0\rangle$. We analyze the duration of the single link entanglement generation T_{SL} of the protocol in Ref. [54], where we account for parallelization of the different entanglement generation steps using results from Refs. [62–64]. We take the ENs time-scale as dominated by the ion-emission and the BBs by the quantum and classical communication time, estimated by twice the light propagation time from the nodes to the heralding station. The BB generation rate is directly enhanced by multiplexing via N_{BB} modes. Additionally, the duration scales with the inverse of the first and second swap probability (which are limited by the memory efficiency and given in Ref. [54]).

The fundamental link generation corresponds to a single-click protocol, which is known to suffer from "vacuum growth" where the memories end up in the joint

vacuum state [31, 32]. This aligns with our model where in contrast to the “two-photon” component $D_{1,1}$, the “vacuum” component $D_{0,0}$ always appears with a significant probability in the presence of photon loss. Therefore, we propose to follow the generation of two fundamental links, by local CNOTs between the ions of two fundamental links. Post-selecting on the controlled ions each being in state $|1\rangle$ heralds success with probability $P_P = 2D_{1,0}D_{0,1} + 2D_{0,0}D_{1,1}$ and the state of the remaining pair takes the same form as Eq. (5). However, purification changes the state according to $\alpha_{\text{pur}} = \frac{\alpha^2}{P_P}$ and $D_{k,l}^{\text{pur}} = \frac{D_{k,l}D_{1-k,1-l}}{P_P}$, so that both $D_{0,0}^{\text{pur}}$ and $D_{1,1}^{\text{pur}}$ can be reduced by lowering the emission probabilities $|\alpha_1|^2, |\beta_1|^2, |\gamma_1|^2$ if the dark-count rate p_d/T is sufficiently small, since the leading contributions of $D_{1,1}$ are proportional to these. Assuming that the two fundamental links are generated sequentially, the complete average duration including purification is $2T_{\text{SL}}/P_P$.

With the above model, we evaluate the average duration for the entanglement of ion-ion pairs. For a target Bell state fidelity of $F = 0.99$ for internal efficiencies of $\eta_I = 0.9$ and assuming the pulses to be matched, constant and of realistic durations $1/|\nu(t_c)|^2 = 10/|\mu(t_c)|^2 = 10 \mu\text{s}$ [20, 47]. This corresponds to matching the ion with 10 time-bins and having a time-bin duration of $10T_c$ [24]. In terms of the internal efficiencies we use $\eta_A = \eta_I, \eta_B = \eta_I$ (frequency conversion), and $\eta_{BB} = \eta_I e^{-L/nL_{\text{att}}}$ with $n = 4(2)$ with(out) a repeater and $L_{\text{att}} = \frac{10}{0.2 \log 10} \text{ km}$. Optimizing with respect to the emission probabilities $|\alpha_1|^2, |\beta_1|^2, |\gamma_1|^2$ [54, 59, 65], we find the results shown in Fig. 3. For comparison, we also include the time for direct ion-ion entanglement. Due to the longer ion pulses, direct generation only works for a shorter distance for the same dark-count rate. We observe a speedup of around an order of magnitude thanks to the multiplexing of the hybrid architecture compared to direct ion-ion links. While this does not saturate the ideal speedup of the channel capacity due to the additional probabilistic steps and intrinsic losses, it provides a significant speed-up compared to the BB less case. For all protocols included in the figure, the entangled state is between ions, and thus the advanced trapped-ion capabilities are available, including deterministic entanglement swaps to extend the range.

If the target fidelity is relaxed to $F = 0.9$, our protocol including a central multi-mode memory repeater achieves an average entanglement generation rate exceeding 1 Hz over a distance of 500 km (for the same parameters). Finally, while we here considered a single-click protocol with purification of the ions, we show in Ref. [54], for high memory efficiencies, we can achieve similar rates between using a double-click approach to create spin-photon entanglement between the ion and a dual rail setup. This relaxes the phase stability requirements on the ions and omits the need of an extra purification step. Therefore, we consider this approach more viable in the presence of

highly efficient photonic memories, whereas the protocol investigated in this work is more suitable for near-term memories.

Conclusion We developed a protocol uniting trapped ions with atomic ensemble systems. At the core of our protocol is a novel approach to link spontaneous parametric down conversion sources and absorptive memories with trapped ions, i.e., broad-band ensemble systems with single narrow-band quantum emitters. This enables the use of multiplexing of ensemble based approaches combined with the more advanced gate sets and deterministic entanglement swaps of trapped ions for further processing of the information. Our approach shows a significant speedup and provides better resilience regarding dark counts compared to direct ion-ion entanglement generation. Moreover, the SPDC matching approach can be extended to couple other narrow-band systems to broadband memories, thereby also enabling inter-connectivity between those systems.

We thank T. E. Northup, H. de Riedmatten, S. D. C. Wehner, M. van Hooft, N. Sangouard, P. Cussenot, B. Grivet, S. Grandi, and A. Das for fruitful discussions. This work was funded by the European Union’s Horizon Europe research and innovation programme under grant agreement No. 101102140 – QIA Phase 1. Funded by the European Union. Views and opinions expressed are however those of the authors only and do not necessarily reflect those of the European Union or European Commission. Neither the European Union nor the granting authority can be held responsible for them. BT, ERH and ASS acknowledge the support of Danmarks Grundforskningsfond (DNRF Grant No. 139, Hy-Q Center for Hybrid Quantum Networks).

* benedikt.tissot@nbi.ku.dk

† anders.sorensen@nbi.ku.dk

- [1] H. J. Kimble, The quantum internet, *Nature* **453**, 1023 (2008).
- [2] S. Wehner, D. Elkouss, and R. Hanson, Quantum internet: a vision for the road ahead, *Science* **362**, eaam9288 (2018).
- [3] A. K. Ekert, Quantum cryptography based on Bell’s theorem, *Phys. Rev. Lett.* **67**, 661 (1991).
- [4] A. Acín, N. Brunner, N. Gisin, S. Massar, S. Pironio, and V. Scarani, Device-independent security of quantum cryptography against collective attacks, *Phys. Rev. Lett.* **98**, 230501 (2007).
- [5] N. Gisin and R. Thew, Quantum communication, *Nat. Photonics* **1**, 165 (2007).
- [6] S. Pirandola, U. L. Andersen, L. Banchi, M. Berta, D. Bunandar, R. Colbeck, D. Englund, T. Gehring, C. Lupo, C. Ottaviani, J. L. Pereira, M. Razavi, J. S. Shaari, M. Tomamichel, V. C. Usenko, G. Vallone, P. Villoresi, and P. Wallden, Advances in quantum cryptography, *Adv. Opt. Photonics* **12**, 1012 (2020).
- [7] W. Wasilewski, K. Jensen, H. Krauter, J. J. Renema,

M. V. Balabas, and E. S. Polzik, Quantum noise limited and entanglement-assisted magnetometry, *Phys. Rev. Lett.* **104**, 133601 (2010).

[8] C. Cassens, B. Meyer-Hoppe, E. Rasel, and C. Klempf, Entanglement-enhanced atomic gravimeter, *Phys. Rev. X* **15**, 011029 (2025).

[9] D. Cuomo, M. Caleffi, and A. S. Cacciapuoti, Towards a distributed quantum computing ecosystem, *IET Quantum Communication* **1**, 3 (2020).

[10] J. S. Bell, On the einstein podolsky rosen paradox, *Phys. Phys. Fiz.* **1**, 195 (1964).

[11] J. F. Clauser, M. A. Horne, A. Shimony, and R. A. Holt, Proposed experiment to test local hidden-variable theories, *Phys. Rev. Lett.* **23**, 880 (1969).

[12] B. Hensen, H. Bernien, A. E. Dréau, A. Reiserer, N. Kalb, M. S. Blok, J. Ruitenberg, R. F. L. Vermeulen, R. N. Schouten, C. Abellán, W. Amaya, V. Pruneri, M. W. Mitchell, M. Markham, D. J. Twitchen, D. Elkouss, S. Wehner, T. H. Taminiau, and R. Hanson, Loophole-free Bell inequality violation using electron spins separated by 1.3 kilometres, *Nature* **526**, 682 (2015).

[13] M. Giustina, M. A. M. Versteegh, S. Wengerowsky, J. Handsteiner, A. Hochrainer, K. Phelan, F. Steinlechner, J. Kofler, J.-Å. Larsson, C. Abellán, W. Amaya, V. Pruneri, M. W. Mitchell, J. Beyer, T. Gerrits, A. E. Lita, L. K. Shalm, S. W. Nam, T. Scheidl, R. Ursin, B. Wittmann, and A. Zeilinger, Significant-loophole-free test of Bell's theorem with entangled photons, *Phys. Rev. Lett.* **115**, 250401 (2015).

[14] S. Storz, J. Schär, A. Kulikov, P. Magnard, P. Kurpiers, J. Lütfolf, T. Walter, A. Copetudo, K. Reuer, A. Akin, J.-C. Besse, M. Gabureac, G. J. Norris, A. Rosario, F. Martin, J. Martinez, W. Amaya, M. W. Mitchell, C. Abellán, J.-D. Bancal, N. Sangouard, B. Royer, A. Blais, and A. Wallraff, Loophole-free Bell inequality violation with superconducting circuits, *Nature* **617**, 265 (2023).

[15] C.-W. Chou, J. Laurat, H. Deng, K. S. Choi, H. de Riedmatten, D. Felinto, and H. J. Kimble, Functional quantum nodes for entanglement distribution over scalable quantum networks, *Science* **316**, 1316 (2007).

[16] Z.-S. Yuan, Y.-A. Chen, B. Zhao, S. Chen, J. Schmiedmayer, and J.-W. Pan, Experimental demonstration of a bdcz quantum repeater node, *Nature* **454**, 1098 (2008).

[17] Y. Yu, F. Ma, X.-Y. Luo, B. Jing, P.-F. Sun, R.-Z. Fang, C.-W. Yang, H. Liu, M.-Y. Zheng, X.-P. Xie, W.-J. Zhang, L.-X. You, Z. Wang, T.-Y. Chen, Q. Zhang, X.-H. Bao, and J.-W. Pan, Entanglement of two quantum memories via fibres over dozens of kilometres, *Nature* **578**, 240 (2020).

[18] D. L. Moehring, P. Maunz, S. Olmschenk, K. C. Younge, D. N. Matsukevich, L.-M. Duan, and C. Monroe, Entanglement of single-atom quantum bits at a distance, *Nature* **449**, 68 (2007).

[19] L. J. Stephenson, D. P. Nadlinger, B. C. Nichol, S. An, P. Drmota, T. G. Ballance, K. Thirumalai, J. F. Goodwin, D. M. Lucas, and C. J. Ballance, High-rate, high-fidelity entanglement of qubits across an elementary quantum network, *Phys. Rev. Lett.* **124**, 110501 (2020).

[20] V. Krutyanskiy, M. Galli, V. Krcmarsky, S. Baier, D. A. Fioretto, Y. Pu, A. Mazloom, P. Sekatski, M. Canteri, M. Teller, J. Schupp, J. Bate, M. Meraner, N. Sangouard, B. P. Lanyon, and T. E. Northup, Entanglement of trapped-ion qubits separated by 230 meters, *Phys. Rev. Lett.* **130**, 050803 (2023).

[21] H. Bernien, B. Hensen, W. Pfaff, G. Koolstra, M. S. Blok, L. Robledo, T. H. Taminiau, M. Markham, D. J. Twitchen, L. Childress, and R. Hanson, Heralded entanglement between solid-state qubits separated by three metres, *Nature* **497**, 86 (2013).

[22] A. Sipahigil, R. E. Evans, D. D. Sukachev, M. J. Burek, J. Borregaard, M. K. Bhaskar, C. T. Nguyen, J. L. Pacheco, H. A. Atikian, C. Meuwly, R. M. Camacho, F. Jelezko, E. Bielejec, H. Park, M. Lončar, and M. D. Lukin, An integrated diamond nanophotonics platform for quantum-optical networks, *Science* **354**, 847 (2016).

[23] P. C. Humphreys, N. Kalb, J. P. J. Morits, R. N. Schouten, R. F. L. Vermeulen, D. J. Twitchen, M. Markham, and R. Hanson, Deterministic delivery of remote entanglement on a quantum network, *Nature* **558**, 268 (2018).

[24] D. Lago-Rivera, S. Grandi, J. V. Rakonjac, A. Seri, and H. de Riedmatten, Telecom-heralded entanglement between multimode solid-state quantum memories, *Nature* **594**, 37 (2021).

[25] X. Liu, J. Hu, Z.-F. Li, X. Li, P.-Y. Li, P.-J. Liang, Z.-Q. Zhou, C.-F. Li, and G.-C. Guo, Heralded entanglement distribution between two absorptive quantum memories, *Nature* **594**, 41 (2021).

[26] A. Ruskuc, C.-J. Wu, E. Green, S. L. N. Hermans, W. Pajak, J. Choi, and A. Faraon, Multiplexed entanglement of multi-emitter quantum network nodes, *Nature* **639**, 54–59 (2025).

[27] C. D. Bruzewicz, J. Chiaverini, R. McConnell, and J. M. Sage, Trapped-ion quantum computing: Progress and challenges, *Appl. Phys. Rev.* **6**, 021314 (2019).

[28] S. A. Moses, C. H. Baldwin, M. S. Allman, R. Ancona, L. Ascarrunz, C. Barnes, J. Bartolotta, B. Bjork, P. Blanchard, M. Bohn, J. G. Bohnet, N. C. Brown, N. Q. Burdick, W. C. Burton, S. L. Campbell, J. P. Campora, C. Carron, J. Chambers, J. W. Chan, Y. H. Chen, A. Chernoguzov, E. Chertkov, J. Colina, J. P. Curtis, R. Daniel, M. DeCross, D. Deen, C. Delaney, J. M. Dreiling, C. T. Ertsgaard, J. Esposito, B. Estey, M. Fabrikant, C. Figgatt, C. Foltz, M. Foss-Feig, D. Francois, J. P. Gaebler, T. M. Gatterman, C. N. Gilbreth, J. Giles, E. Glynn, A. Hall, A. M. Hankin, A. Hansen, D. Hayes, B. Higashi, I. M. Hoffman, B. Horning, J. J. Hout, R. Jacobs, J. Johansen, L. Jones, J. Karcz, T. Klein, P. Lauria, P. Lee, D. Liefer, S. T. Lu, D. Lucchetti, C. Lytle, A. Malm, M. Matheny, B. Mathewson, K. Mayer, D. B. Miller, M. Mills, B. Neyenhuis, L. Nugent, S. Olson, J. Parks, G. N. Price, Z. Price, M. Pugh, A. Ransford, A. P. Reed, C. Roman, M. Rowe, C. Ryan-Anderson, S. Sanders, J. Sedlacek, P. Shevchuk, P. Siegfried, T. Skripka, B. Spaun, R. T. Sprenkle, R. P. Stutz, M. Swallows, R. I. Tobey, A. Tran, T. Tran, E. Vogt, C. Volin, J. Walker, A. M. Zolot, and J. M. Pino, A race-track trapped-ion quantum processor, *Phys. Rev. X* **13**, 041052 (2023).

[29] P. Wang, C.-Y. Luan, M. Qiao, M. Um, J. Zhang, Y. Wang, X. Yuan, M. Gu, J. Zhang, and K. Kim, Single ion qubit with estimated coherence time exceeding one hour, *Nat. Commun.* **12**, 233 (2021).

[30] M. Riebe, T. Monz, K. Kim, A. S. Villar, P. Schindler, M. Chwalla, M. Hennrich, and R. Blatt, Deterministic entanglement swapping with an ion-trap quantum computer, *Nat. Phys.* **4**, 839 (2008).

[31] N. Sangouard, C. Simon, H. de Riedmatten, and N. Gisin,

Quantum repeaters based on atomic ensembles and linear optics, *Rev. Mod. Phys.* **83**, 33 (2011).

[32] H. K. Beukers, M. Pasini, H. Choi, D. Englund, R. Hanson, and J. Borregaard, Remote-entanglement protocols for stationary qubits with photonic interfaces, *PRX Quantum* **5**, 010202 (2024).

[33] C. Simon, H. de Riedmatten, M. Afzelius, N. Sangouard, H. Zbinden, and N. Gisin, Quantum repeaters with photon pair sources and multimode memories, *Phys. Rev. Lett.* **98**, 190503 (2007).

[34] N. Sinclair, E. Saglamyurek, H. Mallahzadeh, J. A. Slater, M. George, R. Ricken, M. P. Hedges, D. Oblak, C. Simon, W. Sohler, and W. Tittel, Spectral multiplexing for scalable quantum photonics using an atomic frequency comb quantum memory and feed-forward control, *Phys. Rev. Lett.* **113**, 053603 (2014).

[35] A. Ruskuc, C.-J. Wu, J. Rochman, J. Choi, and A. Faraon, Nuclear spin-wave quantum register for a solid-state qubit, *Nature* **602**, 408 (2022).

[36] M. Zhong, M. P. Hedges, R. L. Ahlefeldt, J. G. Bartholomew, S. E. Beavan, S. M. Wittig, J. J. Longdell, and M. J. Sellars, Optically addressable nuclear spins in a solid with a six-hour coherence time, *Nature* **517**, 177 (2015).

[37] M. Businger, L. Nicolas, T. S. Mejia, A. Ferrier, P. Goldner, and M. Afzelius, Non-classical correlations over 1250 modes between telecom photons and 979-nm photons stored in $^{171}\text{Yb}^{3+}:\text{Y}_2\text{SiO}_5$, *Nat. Commun.* **13**, 6438 (2022).

[38] C. Clausen, I. Usmani, F. Bussières, N. Sangouard, M. Afzelius, H. de Riedmatten, and N. Gisin, Quantum storage of photonic entanglement in a crystal, *Nature* **469**, 508 (2011).

[39] E. Saglamyurek, N. Sinclair, J. Jin, J. A. Slater, D. Oblak, F. Bussières, M. George, R. Ricken, W. Sohler, and W. Tittel, Broadband waveguide quantum memory for entangled photons, *Nature* **469**, 512 (2011).

[40] M. Bock, P. Eich, S. Kucera, M. Kreis, A. Lenhard, C. Becher, and J. Eschner, High-fidelity entanglement between a trapped ion and a telecom photon via quantum frequency conversion, *Nat. Commun.* **9**, 1998 (2018).

[41] S. Saha, M. Shalaev, J. O'Reilly, I. Goetting, G. Toh, A. Kalakuntla, Y. Yu, and C. Monroe, High-fidelity remote entanglement of trapped atoms mediated by time-bin photons, *Nat. Commun.* **16**, 2533 (2025).

[42] G. S. Vasilev, D. Ljunggren, and A. Kuhn, Single photons made-to-measure, *New J. Phys.* **12**, 063024 (2010).

[43] P. Farrera, G. Heinze, B. Albrecht, M. Ho, M. Chávez, C. Teo, N. Sangouard, and H. de Riedmatten, Generation of single photons with highly tunable wave shape from a cold atomic ensemble, *Nat. Commun.* **7**, 13556 (2016).

[44] O. Morin, M. Körber, S. Langenfeld, and G. Rempe, Deterministic shaping and reshaping of single-photon temporal wave functions, *Phys. Rev. Lett.* **123**, 133602 (2019).

[45] B. Tissot and G. Burkard, Efficient high-fidelity flying qubit shaping, *Phys. Rev. Research* **6**, 013150 (2024).

[46] P. Cussenot, B. Grivet, B. P. Lanyon, T. E. Northup, H. de Riedmatten, A. S. Sørensen, and N. Sangouard, Uniting quantum processing nodes of cavity-coupled ions with rare-earth quantum repeaters using single-photon pulse shaping based on atomic frequency comb, arXiv:2501.18704 [quant-ph].

[47] M. Meraner, A. Mazloom, V. Krutyanskiy, V. Krcmarsky, J. Schupp, D. A. Fioretto, P. Sekatski, T. E. Northup, N. Sangouard, and B. P. Lanyon, Indistinguishable photons from a trapped-ion quantum network node, *Phys. Rev. A* **102**, 052614 (2020).

[48] S. D. Barrett and P. Kok, Efficient high-fidelity quantum computation using matter qubits and linear optics, *Phys. Rev. A* **71**, 060310 (2005).

[49] K. Nemoto, M. Trupke, S. J. Devitt, A. M. Stephens, B. Scharfenberger, K. Buczak, T. Nöbauer, M. S. Everitt, J. Schmiedmayer, and W. J. Munro, Photonic architecture for scalable quantum information processing in diamond, *Phys. Rev. X* **4**, 031022 (2014).

[50] F. Omlor, B. Tissot, and G. Burkard, Entanglement generation using single-photon pulse reflection in realistic networks, *Phys. Rev. A* **111**, 012612 (2025).

[51] Further probabilistic repeaters would not benefit in the same way from the parallelization, which is why we propose to only use the probabilistic swaps in “fundamental” links and to extend range and complexity of the network beyond the fundamental link using deterministic ion swaps.

[52] L.-M. Duan, M. D. Lukin, J. I. Cirac, and P. Zoller, Long-distance quantum communication with atomic ensembles and linear optics, *Nature* **414**, 413 (2001).

[53] B. Zhao, Z.-B. Chen, Y.-A. Chen, J. Schmiedmayer, and J.-W. Pan, Robust creation of entanglement between remote memory qubits, *Phys. Rev. Lett.* **98**, 240502 (2007).

[54] B. Tissot, S. Maiti, E. R. Hellebek, and A. S. Sørensen, Single and double-click high-rate entanglement generation between distant ions using multiplexed atomic ensembles, arxiv:2511.xxxxx (2025), companion paper.

[55] M. Keller, B. Lange, K. Hayasaka, W. Lange, and H. Walther, Continuous generation of single photons with controlled waveform in an ion-trap cavity system, *Nature* **431**, 1075 (2004).

[56] H. G. Barros, A. Stute, T. E. Northup, C. Russo, P. O. Schmidt, and R. Blatt, Deterministic single-photon source from a single ion, *N. J. Phys.* **11**, 103004 (2009).

[57] E. R. Hellebek, K. Mølmer, and A. S. Sørensen, Characterization of the multimode nature of single-photon sources based on spontaneous parametric down-conversion, *Phys. Rev. A* **110**, 023728 (2024).

[58] V. Krutyanskiy, M. Canteri, M. Meraner, V. Krcmarsky, and B. Lanyon, Multimode ion-photon entanglement over 101 kilometers, *PRX Quantum* **5**, 020308 (2024).

[59] See supplemental material at the end of the arxiv submission for further details on uncorrelated SPDC emission and the optimal emission probabilities leading to the duration in Fig. 3.

[60] J. V. Rakonjac, D. Lago-Rivera, A. Seri, M. Mazzera, S. Grandi, and H. de Riedmatten, Entanglement between a telecom photon and an on-demand multimode solid-state quantum memory, *Phys. Rev. Lett.* **127**, 210502 (2021).

[61] M. Teller, S. Plascencia, C. S. Jachimska, S. Grandi, and H. de Riedmatten, A solid-state temporally multiplexed quantum memory array at the single-photon level, *npj Quantum Information* **11**, 92 (2025).

[62] L. Jiang, J. M. Taylor, and M. D. Lukin, Fast and robust approach to long-distance quantum communication with atomic ensembles, *Phys. Rev. A* **76**, 012301 (2007).

[63] T. Coopmans, S. Brand, and D. Elkouss, Improved analytical bounds on delivery times of long-distance entanglement, *Phys. Rev. A* **105**, 012608 (2022).

- [64] G. Avis, R. Knegjens, A. S. Sørensen, and S. Wehner, Asymmetric node placement in fiber-based quantum networks, *Phys. Rev. A* **109**, 052627 (2024).
- [65] B. Tissot, S. Maiti, E. R. Hellebek, and A. S. Sørensen, The code supporting the findings of this manuscript is provided as ancillary files of ref. [54] (2025).
- [66] P. K. Mogensen and A. N. Riseth, Optim: A mathematical optimization package for Julia, *Journal of Open Source Software* **3**, 615 (2018).

SPDC uncorrelated pairs

To match the SPDC and trapped ions, we considered the weak driving limit for the SPDC in the main text. In this appendix we quantify the meaning of weak driving, link it to the emission of uncorrelated photon pairs and the implications for the model used in the main text. Considering a weakly driven SPDC source, it is unlikely that two emissions happen simultaneously. Here, we quantify the meaning of “weakly driven” as having a small probability to have a photon pair emitted during time-bin duration $T_{\text{TB}} \gg T_c$ (with the correlation time T_c). Thus we write the two-photon component using $G(\vec{t}) = \delta_1 F(t_1, t_3) F(t_2, t_4) + \delta_2 (t_1 \leftrightarrow t_2)$. Normalization of the two-photon wave function leads to $2|\delta_1 + \delta_2|^2 \approx 1$, where we disregarded terms of $\mathcal{O}(T_c/T_{\text{TB}})$.

Additionally, we assume that in the weakly driven case, the photons in a single channel should be uncorrelated (or the emitted photon pairs should be uncorrelated). This corresponds to a $g_2(t, t') \approx 1$ within channel b or to

$$\langle \Psi_b | b^\dagger(t) b(t) | \Psi_b \rangle \approx \frac{\langle \Psi_b | b^\dagger(t) b^\dagger(t') b(t') b(t) | \Psi_b \rangle}{\langle \Psi_b | b^\dagger(t') b(t') | \Psi_b \rangle}, \quad (6)$$

for $|t - t'| \gg T_c$. The vacuum part of the state [i.e., the term $\propto \beta_0$ in Eq. (2)] does not contribute to either side of Eq. (6). Evaluating the expectation values of Eq. (6) leads to

$$|\beta_1|^2 + 2|\beta_2|^2 = \frac{2|\beta_2|^2}{|\beta_1|^2 + 2|\beta_2|^2}, \quad (7)$$

which is solved by $2|\beta_{2,\pm}|^2 = \frac{1}{2} - |\beta_1|^2 \pm \sqrt{\frac{1}{4} - |\beta_1|^2} \approx \begin{cases} 1 - 2|\beta_1|^2 - |\beta_1|^4 \\ |\beta_1|^4 \end{cases}$. The approximation holds for small β_1 and we expect $|\beta_2|^2 < |\beta_1|^2$, therefore we use $2|\beta_2|^2 \approx |\beta_1|^4$ for small emission probabilities (or weak drives).

Additional details on the optimization

The emission probabilities corresponding to the results in Fig. 3 of the main text are displayed in Fig. 4. For the protocol proposed in the main text, we numerically optimize the emission probabilities $|\alpha_1|^2$, $|\beta_1|^2$, and $|\gamma_1|^2$ using “Optim.jl” [66]. For the direct ion-ion approach, we use 10000 exponentially spaced samples for the ion emission probability $|\alpha_1|^2$ between 10^{-1} and 10^{-6} , decreasing until we find the first value that satisfies the fidelity constraint, while for the proposed protocol, we perform a numerical optimization of all three emission probabilities. We provide the implementation in Ref. [65].

To further understand the emission probabilities, we estimate the optimal asymmetry in the generated link

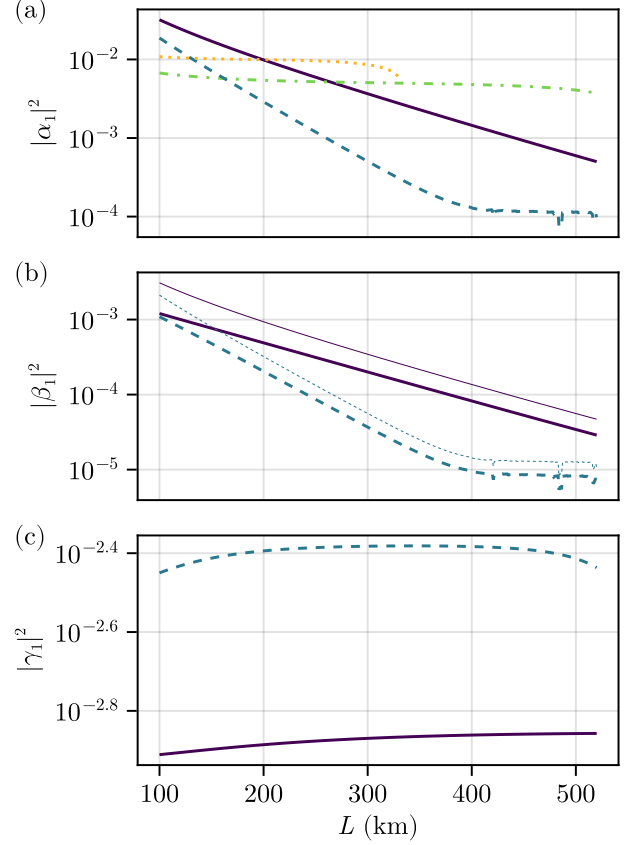


FIG. 4. Optimal emission probabilities corresponding to the results displayed in Fig. 3 of the main text. The line styles encode the protocols and follow Fig. 3 of the main text. The thin lines in (b) correspond to the semi-analytic approach [see Eq. (8)]. In panel (a) we show the emission probability of the ions $|\alpha_1|^2$, in (b) of the SPDC connecting memory and ions in the end-nodes $|\beta_1|^2$ and in (c) of the SPDC within the BB $|\gamma_1|^2$.

at the edge-nodes, quantified by the angle θ . To this end, we analytically maximize the leading-order product $\mathbf{P}_{S1}\mathbf{P}_{S2}\alpha$, which is 0th order in emission amplitudes. For completeness we note that the leading orders success probabilities of the first and second swap operations are $\mathbf{P}_{S1} \approx \frac{\eta_m}{2} + \eta_m(1 - \eta_m) \frac{\tan^2 \theta}{\eta_m + \tan^2 \theta}$ and $\mathbf{P}_{S2} \approx \frac{(3+X)(1-\eta_m)\sin^2 \theta + 2\eta_m \cos^2 \theta}{\eta_m + 3(1-\eta_m)\sin^2 \theta} \frac{\eta_m \sin^2 \theta}{\eta_m + X(1-\eta_m)\sin^2 \theta}$, where $X = 1(3)$ without (with) the central repeater. For more details see Ref. [54]. Finally, for the leading order off-diagonal density matrix element we have $\alpha \propto \frac{1}{2} \cos^2 \theta \sin^2 \theta \frac{\eta_m}{\eta_m + 3(1-\eta_m)\sin^2 \theta} \frac{\eta_m}{\eta_m + X(1-\eta_m)\sin^2 \theta}$.

Analytically we find a maximum of $\mathbf{P}_{S1}\mathbf{P}_{S2}\alpha$ with regard to θ if θ satisfies

$$\tan^2 \theta = \frac{\eta_m}{\sqrt{\eta_m + (1 - \eta_m)X}}. \quad (8)$$

Note that the (ideal) final state remains symmetric, because the asymmetry of the EN states contributes evenly on both sides (i.e., symmetric). A comparison of the

emission probabilities predicted using the semi-analytical approach and the numeric approach is given in Fig. 4.